2014

Aerosol microphysical impact on summertime convective precipitation in the Rocky Mountain region

Trude Eidhammer
National Center for Atmospheric Research

Mary C. Barth
National Center for Atmospheric Research

Markus D. Petters
North Carolina State University

Christine Wiedinmyer
National Center for Atmospheric Research

Anthony J. Prenni
Colorado State University

AGU PUBLICATIONS

JGR

Journal of Geophysical Research: Atmospheres

RESEARCH ARTICLE
10.1002/2014JD021883

Key Points:
- WRF-Chem underestimate aerosol organic fraction without new particle formation
- Homogeneous increases in aerosol concentration decrease precipitation
- Heterogeneous increases in aerosol concentration increase precipitation

Correspondence to:
T. Eidhammer,
trude@ucar.edu

Citation:
Eidhammer, T., M. C. Barth, M. D. Petters, C. Wiedinmyer, and A. J. Prenni (2014), Aerosol microphysical impact on summertime convective precipitation in the Rocky Mountain region, *J. Geophys. Res. Atmos.*, *119*, 11,709–11,728, doi:10.1002/2014JD021883.

Received 10 APR 2014
Accepted 17 SEP 2014
Accepted article online 18 SEP 2014
Published online 16 OCT 2014

Aerosol microphysical impact on summertime convective precipitation in the Rocky Mountain region

Trude Eidhammer[1], Mary C. Barth[1], Markus D. Petters[2], Christine Wiedinmyer[1], and Anthony J. Prenni[3,4]

[1]National Center for Atmospheric Research, Boulder, Colorado, USA, [2]Department of Marine Earth and Atmospheric Sciences, North Carolina State University at Raleigh, Raleigh, North Carolina, USA, [3]Department of Atmospheric Science, Colorado State University, Fort Collins, Colorado, USA, [4]Now at Air Resources Division, National Park Service, Lakewood, Colorado, USA

Abstract We present an aerosol-cloud-precipitation modeling study of convective clouds using the Weather Research and Forecasting model fully coupled with Chemistry (WRF-Chem) version 3.1.1. Comparison of the model output with measurements from a research site in the Rocky Mountains in Colorado revealed that the fraction of organics in the model is underpredicted. This is most likely due to missing processes in the aerosol module in the model version used, such as new particle formation and growth of secondary organic aerosols. When boundary conditions and domain-wide initial conditions of aerosol loading are changed in the model (factors of 0.1, 0.2, and 10 of initial aerosol mass of SO_4^{-2}, NH_4^+, and NO_3^-), the domain-wide precipitation changes by about 5%. Analysis of the model results reveals that the Rocky Mountain region and Front Range environment is not conducive for convective invigoration to play a major role, in increasing precipitation, as seen in some other studies. When localized organic aerosol emission are increased to mimic new particle formation, the resulting increased aerosol loading leads to increases in domain-wide precipitation, opposite to what is seen in the model simulations with changed boundary and initial conditions.

1. Introduction

Aerosols play an important role in cloud formation, as they act as seeds for droplet and ice crystal formation. How efficient the aerosols are in influencing cloud formation processes depends on their composition, size, and number concentration. Changes in these aerosol properties affect cloud droplet number concentrations and lead to changes in cloud albedo [*Twomey*, 1974], and cloud fraction and lifetime [*Albrecht*, 1989], and subsequently impact the radiative balance of the atmosphere. Thus, aerosols impose an indirect effect on climate through changes in cloud properties. Modeling studies suggest that aerosol indirect effects can cause negative global radiative forcing [e.g. *Lohmann et al.*, 2000; *Ghan et al.*, 2001; *Chen and Penner*, 2005; *Kristjánsson*, 2002; *Penner et al.*, 2006] thus having significant implications for understanding climate impacts.

Aerosol-cloud interactions have the potential to change the microphysical properties of the clouds. Efficiency of precipitation might be enhanced or decreased, imposing a possible effect on the hydrological cycle [e.g., *Li et al.*, 2011; *Rosenfeld et al.*, 2008]. For warm (liquid-only) clouds, an increase in aerosol number concentration will typically increase droplet number concentration, thus reducing the droplet size. This reduction of droplet size will slow down and delay the onset of precipitation. However, the picture is more complex when considering convective clouds. These are typically mixed-phase clouds where ice microphysics complicates the estimation of aerosol effects.

Several modeling experiments have been conducted to determine the effect aerosols have on precipitation (among other factors) in mixed-phase convective clouds. These studies can be divided into single versus multicell and ensemble cloud studies using 2- and 3-D models. The review paper by *Tao et al.* [2012] compiles several different studies that show that increases in aerosols or cloud droplet number concentrations can lead to increases or decreases in precipitation amounts. Some studies suggest that in mixed phase clouds, when more numerous but smaller droplets cross the freezing level, more drops are available for freezing, thus enhancing the latent heat release [e.g., *Andreae et al.*, 2004; *Rosenfeld et al.*, 2008]. The increase in latent

heating invigorates the cloud (i.e., increases the upward transport), allowing for increases in precipitation amount. For this invigoration to occur, cloud base temperature typically is warmer than about 15°C [*Rosenfeld et al.*, 2008; *Li et al.*, 2011].

Several environmental parameters also influence the sign and magnitude of aerosol effects on precipitation. In environments with low wind shear, precipitation amount is typically enhanced with increases in aerosol (droplet) concentrations, while in strong wind shear the precipitation amount is suppressed [*Fan et al.*, 2009]. *Lebo and Morrison* [2014] attributed this to the cold pool weakening as aerosol concentrations increased. The cold pool weakens due to reduced rain evaporation from fewer but larger raindrops in a more polluted environment. For low wind shear, the balance between the cold pool strength and the low wind shear becomes even more balanced and optimal for convective mass flux when the cold pool weakens. While in strong wind shear, reducing the cold pool strength reduces the balance between cold pool strength and high wind shear strength. Further, *Khain et al.* [2008] and *Khain* [2009] concluded that increases in aerosol concentrations usually decreased precipitation amount in isolated convective clouds in rather dry environments, while in more humid environments, increases in aerosol concentrations can increase precipitation amount. *Khain et al.* [2008] explained the differences seen between wet and dry environment by that in humid air, the condensation gain is larger than the condensation loss when cloud condensation nuclei (CCN) concentrations are increased, while in dry air the condensation gain is less than the evaporation when CCN concentrations are increased. Beyond humidity, wind shear, and cloud/storm type, the convective available potential energy (CAPE) is another parameter thought to play a factor in how precipitation changes with changes in aerosol concentrations. *Lee et al.* [2008] and *Ntelekos et al.* [2009] found that in cases with high aerosol loading, high wind shear, and high CAPE, increased aerosol loadings typically lead to an increase in precipitation.

The drawback of using 2-D idealized model setups to evaluate aerosol-cloud interactions is that the dynamical impacts on the mesoscale from changes in concentrations of aerosols are not necessarily included. For example, when considering the dynamical impact, the entire system can act as a buffer [*Stevens and Feingold*, 2009] and the feedback from the dynamics relaxes any perturbations back to the base state [*Morrison and Grabowski*, 2013], reducing any impact aerosols have on the clouds. This buffering makes it difficult to determine the role aerosols have on the microphysics of clouds.

Recently, an increasing number of studies have investigated aerosol impacts on precipitation using 3-D cloud-resolving models over longer time scales with more detailed microphysics. These studies indicate both increases or decreases in precipitation amount resulting from increases in aerosol concentration that can serve as CCN [e.g. *Lynn et al.*, 2005; *Seifert and Beheng*, 2006; *van den Heever et al.*, 2006; *Ntelekos et al.*, 2009; *Igel et al.*, 2013; *Thompson and Eidhammer*, 2014]. Some of these studies consider isolated cloud systems, and the percentage difference in precipitation from clean to polluted cases is comparable to those found in 2-D modeling studies. In contrast, *Seifert et al.* [2012], *Morrison and Grabowski* [2011], and *van den Heever et al.* [2011] have shown that the storm integrated change in precipitation due to changes in aerosol number concentrations are very small ($<$10%) when averaged over time and space.

Finally, we also note that *Lebo and Seinfeld* [2011] found that using a bulk microphysical scheme resulted in different cumulative precipitation amount when CCN concentration were changed, compared to when using a bin scheme. With everything else being the same, for an idealized 3-D simulation, they found that using a bulk scheme produced slightly more cumulative precipitation when CCN number concentrations were increased, while the precipitation was reduced with a bin scheme. They found that all changes in precipitation were related to changes in condensed water and subsequently the competition between evaporation/sublimation and sedimentation.

In this paper, we investigate aerosol impacts on cloud droplets and precipitation in summer convective clouds over the Rocky Mountain region of Colorado. The water resources and ecosystems in this semiarid region are highly dependent on the amount and location of precipitation. While most of the Colorado River streamflow is from snowmelt, a substantial portion of precipitation in the Rocky Mountains is also from convective storms occurring during the North American monsoon in July and August. To study the susceptibility of the summer convection over Colorado to aerosol microphysics, we conduct our study as part of the Bio-hydro-atmosphere interactions of Energy, Aerosols, Carbon, H_2O, Organics, and Nitrogen (BEACHON) program [*Ortega et al.,* 2014]. The goal of the BEACHON program is to increase the understanding of biogenic trace gases and particulate matter and link them to the carbon and water cycles through

observations and modeling. The BEACHON project has built an infrastructure for long-term measurements at the Manitou Experimental Forest (MEF) just northwest of Colorado Springs, Colorado (39°06′02″N, 105°05′45″W, 2286 m above sea level). There, meteorological, chemical, and aerosol measurements are regularly collected. In addition, a few specific field campaigns have been completed, in 2010 BEACHON Rocky Mountain Organic Carbon Study (ROCS) and in 2011 BEACHON Rocky Mountain Biogenic Aerosol Study (RoMBAS) [e.g., *Ortega et al.*, 2014]. In 2008, the Southern Rocky Mountains Summer Study (SRM08) was conducted from July to September to provide initial meteorological, aerosol (CCN, condensation nuclei (CN), ice nuclei (IN), and aerosol size distributions), and chemical measurements for identifying scientific questions for the later field campaigns (i.e., BEACHON ROCS and RoMBAS). Here we show results from a 3 day 3-D modeling study coinciding with a time period during SRM08. The model is evaluated with measured hygroscopicity and further used to investigate aerosol effects on precipitation in the study region, as well as how well the modeled CCN properties compare with the observations.

After describing the cloud chemistry model and aerosol measurements (section 2), we evaluate the model results with the available SRM08 aerosol observations at the MEF site (section 3). Then we investigate aerosol-cloud-precipitation effects (section 4). We first examine the regional effect of changed aerosol loading by modifying the initial and lateral boundary aerosol loading. Then, we examine the impact of including biogenic organic aerosol emissions (which are not included in the first set of simulations) on clouds and precipitation.

2. Model and Instrument Description

2.1. Aerosol Observations

During the SRM08 campaign, size-resolved CCN measurements were taken using the same instruments and setup as described by *Petters et al.* [2007, 2009]. The instruments were housed in the climate-controlled Mobile Air Quality Laboratory (sponsored by National Park Service). The setup consists of a differential mobility analyzers (DMAs; TSI 3071), a condensation particle counter (CPC), and a cloud condensation nuclei counter [*Roberts and Nenes*, 2005]. The DMA is used to size select the dried and charge equilibrated aerosol prior to exposing the aerosol to a constant supersaturation inside the CCN instrument. Stepping through a series of mobility diameters and referencing to the CPC, CN, and CCN size distributions are obtained. The raw CCN and CN response curves are inverted to correct for the presence of multiply charged particles [*Petters et al.*, 2009]. Taking the ratio of CCN to CN results in an activation spectrum, for which the activation diameter is defined as the threshold size where 50% of the particles serve as CCN. The activation diameter (D50) is used together with the instrument supersaturation and assumed constant temperature (298 K) and surface tension (0.072 J m^{-2}) to compute the hygroscopicity parameter according to the algorithm described in *Petters and Kreidenweis* [2007]. The CCN measurements were conducted performing sequential size scans at supersaturation (S) ~0.14, 0.41, 0.59, and 0.78%, and these measurements were collected continuously from 27 July to 9 August. *Levin et al.* [2012] used a similar setup to measure the annual cycle of CCN concentrations at the same site (from spring 2010 through spring 2011). Further calibration procedures to ensure correct sizing and assignment of instrument supersaturations are provided in detail by *Petters et al.* [2009] and *Levin et al.* [2012].

In general, the measurement technique permits the reconstruction of the aerosol size distribution and particle number concentration. Unfortunately, we did not verify that the integral of the inverted size distribution accurately reflects the actual CN number concentration before or during SRM08. These tests would have required an assessment of particle losses in the inlet and DMA, verification of charging efficiencies in the neutralizer, and full characterization of the kernel function accounting for transfer through the DMA entering the inversion algorithm [*Petters et al.*, 2009] for the assigned bin resolution [*Nguyen et al.*, 2014]. For this reason total CN and CCN concentrations from size distribution integration are not available for SRM08. However, concentration-independent measures such as the shape of the size distribution, the CCN activated fraction, and the hygroscopicity parameter κ could be estimated accurately.

2.2. Model Description

The model used in this study is the Weather Research and Forecasting (WRF) model [*Skamarock et al.*, 2008] coupled with chemistry (WRF-Chem) [*Grell et al.*, 2005; *Fast et al.*, 2006], version 3.1.1, which is an online chemistry model where the chemistry and constituent transport are calculated simultaneously with the meteorology. We use the Carbon-Bond Mechanism version Z (CBMZ) [*Zaveri and Peters*, 1999] for the chemistry,

Table 1. Model Configuration

Setting	Description
Model	WRF-Chem V3.1.1
Horizontal grid boxes	273 × 273
Horizontal grid resolution	3 km
Vertical levels	28 (top at 100 mbar)
Physical and chemical time step	15 s
Initial and lateral boundary conditions	32 km North American Regional Reanalysis (NARR)
Cloud microphysics	Purdue Lin bulk microphysics, with droplet activation linked to aerosols
Shortwave radiation	Goddard[a]
Longwave radiation	Rapid Radiative Transfer Model (RRTM)[b]
Land surface physics	Noah land surface model[c]
Planetary boundary layer physics	YSU[d]
Aerosol module	MOSAIC
Gas module	CBMZ
Chemical initial and lateral boundary conditions	MOZART-4
Anthropogenic emissions	EPA 2005 National Emissions Inventory
Biogenic emissions	MEGAN

[a] *Chou and Suarez* [1994].
[b] *Mlawer et al.* [1997].
[c] *Chen et al.* [1996], *Chen and Dudhia* [2001], and *Chen* [2005].
[d] *Hong et al.* [2006].

which has 53 trace gases and 132 chemical reactions and is appropriate for describing the chemistry occurring in remote to more urban regions. We represent aerosols with the Model for Simulating Aerosol Interactions and Chemistry (MOSAIC) for the aerosol species [*Zaveri et al.*, 2008]. MOSAIC is a bin scheme with optional four or eight size bins and with eight different aerosol components: ammonium (NH_4^+), sodium (Na^+), sulfate (SO_4^{2-}), nitrate (NO_3^-), chloride (Cl^-), organic carbon (OC), black carbon (BC), and other inorganic species (OIN, which contains mineral dust from wind erosion and particles containing iron, calcium, aluminum, etc., from anthropogenic sources). In the WRF-Chem version 3.1.1 MOSAIC aerosol module, homogeneous binary nucleation of H_2SO_4-H_2O is included [*Wexler et al.,* 1994], while formation of new organic particles and the production of secondary organic aerosols are not included, limiting the amount of organic aerosols accounted for. Further, the mineral dust emission, which is placed into the OIN category, is based on *Shaw et al.* [2008]. This scheme includes a vegetation mask parameter, α, which allows the mineral dust emission to be dependent on the amount of vegetation on a given surface type. For this particular study, we applied α values for grassland, shrubland, and savanna of 0.0028, 0.0085, and 0.005, respectively. Note that since α is based on regional-specific data, this parameter is highly tunable.

The Environmental Protection Agency (EPA) 2005 National Emissions Inventory was used to define anthropogenic emissions. The 2008 emissions inventory shows that SO_2 emissions decrease by 6% and particulate matter 2.5 μm ($PM_{2.5}$) by 80% in Colorado compared to the 2005 emissions inventory. In section 4.3, we discuss the potential effects of the 2005 emissions scenario has on the model-observation comparison. The biogenic emissions are determined by the Model of Emissions of Gases and Aerosols from Nature (MEGAN) version 2.04 [*Guenther et al.*, 2006], which was run within the model framework so that local temperatures and sunlight affect the magnitude of the emissions. The chemical initial and boundary conditions came from the Model for Ozone and Related Chemical Tracers (MOZART-4) global chemical transport model [*Emmons et al.*, 2010]. Meteorology initial and boundary conditions were from the 32 km North American Regional Reanalysis (NARR) [*Mesinger et al.*, 2006]. Other parameters in the modeling configuration are listed in Table 1.

One of the primary objectives of this study is to estimate potential aerosol effects on precipitation as the aerosols act as CCN. To investigate these interactions, droplet activation must be coupled to aerosols. In WRF-Chem version 3.1.1, the only microphysics option available for coupling droplet activation to aerosols is the Purdue Lin scheme [*Lin et al.*, 1983]. This is a bulk one-moment microphysics scheme, but with aerosol dependent droplet formation specific for WRF-Chem included [*Chapman et al.*, 2009]. Thus, the scheme is two-moment in regards to droplets (prediction and advection of mass and number concentration). The droplet activation is based on the parameterization developed by *Abdul-Razzak and Ghan* [2002], and the droplet number

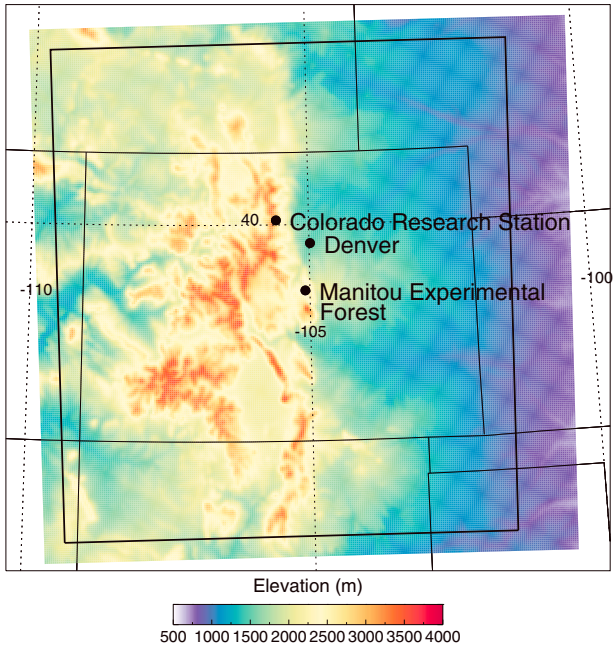

Figure 1. Modeling domain (colored area), showing the terrain and location of the Manitou Experimental Forest site. Black framing indicates the analysis domain.

concentrations are now treated as prognostic variables following *Ghan et al.* [1997]. We note that the droplet activation scheme by *Abdul-Razzak and Ghan* [2002] assumes droplet activation only at the cloud base, while it has been shown that secondary nucleation of droplets can be important in deep convective clouds when supersaturation generation is stronger than the vapor depletion due to growth of hydrometeors [*Pinsky and Khain*, 2002; *Segal et al*., 2003; *Heymsfield et al*., 2009; *Ghan et al*., 2011]. For simplification, the aerosols are assumed to be internal mixtures (i.e., all individual aerosol particles are made up of the same mixture of chemical components). Measurements at the MEF site during BEACHON-RoMBAS support the assumption of an internally mixed aerosol [*Levin et al*., 2014]. To allow droplet number concentration to impact rain formation, the autoconversion parameterization by *Liu et al.* [2005] was implemented [*Chapman et al*., 2009]. Primary ice formation due to ice nuclei is not yet included in any microphysics schemes for use in WRF-Chem. Therefore, the modeled aerosols only have a direct impact on droplet formation in our simulations and not on ice nucleation. It is unclear if changing IN concentration in our simulations would lead to changes in precipitation. For example, *Fan et al.* [2010] found that changes in IN had little impact on convective strength in their simulations of tropical convective clouds. However, *van den Heever et al.* [2006] found that increasing IN in simulation of convective clouds over Florida lead to increasing precipitation.

To isolate the effect aerosols have on precipitation from direct aerosol effects (scattering and absorption), the aerosols are not allowed to affect radiation feedbacks in our simulations. Thus, aerosol scattering or absorption will not change the temperature profiles: any changes observed in the model output are the result only of the indirect effects from aerosols impacting droplet formation. However, leaving out the direct effect is in accordance with previous modeling studies that prescribe CCN or droplet concentrations (and do not rely on the aerosol activation schemes) allowing us to compare our results to these previous studies.

2.3. Model Configuration

The model is set up with the MEF site in the center of the domain. We use a horizontal grid consisting of 273 by 273 points with 3 km grid spacing, resulting in a domain area of $819 \times 819\ km^2$ (Figure 1, with the black box indicating the analysis domain). The model top is set at 100 mbar and has 28 vertical layers, where the vertical grid spacing is ~60 m near the surface in the planetary boundary layer, ~300 m above the boundary layer, and ~700 m near the tropopause (~12 km). The physical and chemical processes and the calculations of biogenic emissions all used a 15 s time step (this information is also available in Table 1).

All simulations are run for 3 days (2 August, 12 UTC to 5 August, 12 UTC), and we use 12 h as spin-up time. A 12 h spin-up time should be sufficient, based on *Zhang et al.* [2009], who found that with WRF-Chem simulation with 3 km resolution over Mexico City (surrounded by high-elevation mountains), spin-up times of 6, 12, and 24 h did not produce large differences for surface concentrations of chemical species. The modeled time period is in the middle of BEACHON-SRM 2008 campaign when CCN measurements were collected and precipitation occurred over the region, although not at the MEF site itself. Four different aerosol-cloud-precipitation assessment simulations were initially performed. The first run, or the Control run, included initial and boundary conditions from MOZART-4. Three additional sensitivity simulations were performed, for which the initial and boundary condition of aerosol mass concentrations of SO_4^{-2}, NH_4^{+}, and $NO_3^{-}$are changed as follows:

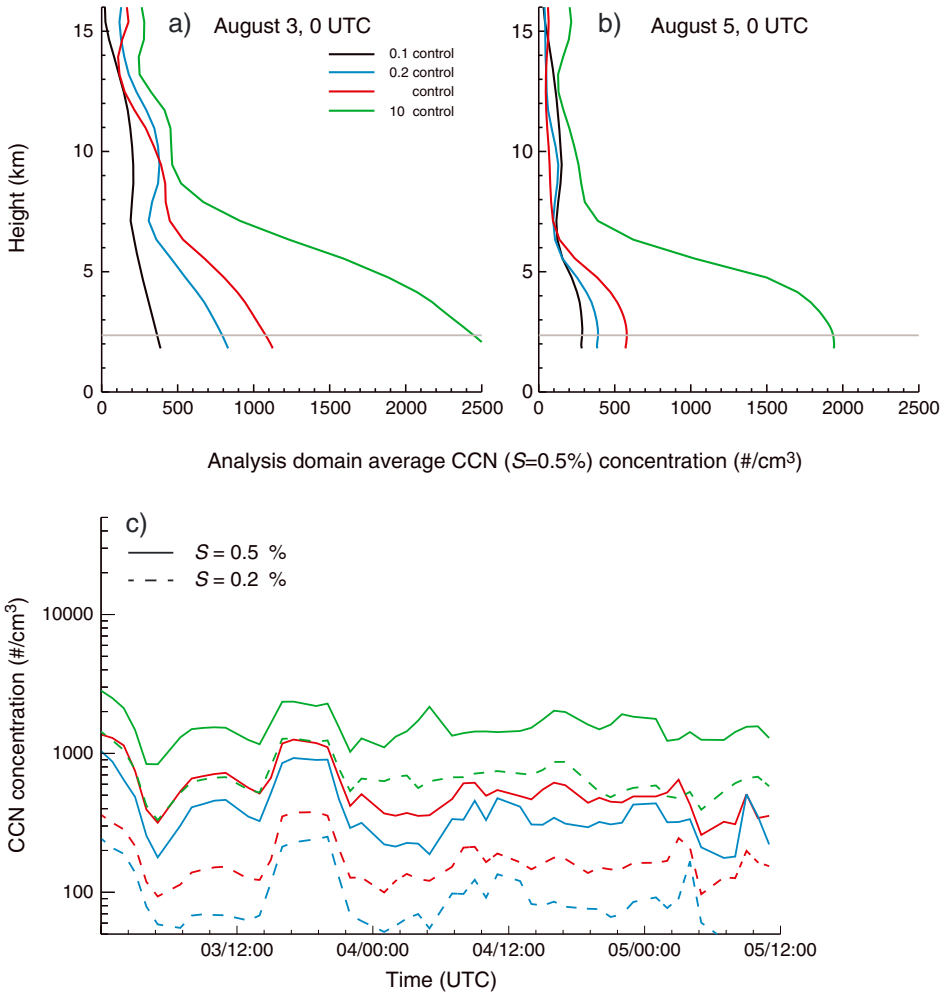

Figure 2. Analysis of domain-wide averaged CCN concentrations ($S = 0.5\%$) as a function of approximate height above sea level; (a) 3 August, 00 UTC (2 August, 18 MDT) and (b) 5 August 5 00 UTC (4 August, 18 MDT). Grey lines indicate height of the MEF site. (c) Time series of CCN concentrations at the lowest model level at the MEF site.

0.1 × Control: aerosol mass concentrations are reduced by a factor of 10, 0.2 × Control: aerosol mass concentrations are reduced by a factor of 5, and 10 × Control: aerosol mass concentrations are increased by a factor of 10.

In all cases, aerosol species are divided into eight size bins (0.039–0.078, 0.078–0.156, 0.156–0.313, 0.313–0.625, 0.625–1.25, 1.25–2.5, 2.5–45.0, and 5.0–10 μm in diameter). The mass in all size bins for the species that are changed is altered by the same factor. Figures 2a and 2b shows the analysis-domain average CCN number concentration at supersaturation, $S = 0.5\%$ as a function of height above sea level at 3 August, 00 UTC (12 h into the simulations) and 5 August, 00 UTC. A tenfold increase or decrease in aerosol mass might seem high, but they are only applied to a subset of the aerosols, and only at the initial time step, but at the boundaries throughout the simulation. Figure 2 shows that the aerosol concentration changes by 2.5–4 times after 24 h simulation when the 10 × Control is applied to the initial and boundary conditions. Figure 2c shows a time series of the modeled CCN concentrations ($S = 0.2$ and 0.5%) at the MEF site. Note that we use the average of the nine nearest grid boxes (i.e., 3 by 3) to the MEF site to calculate the concentrations at the site. The aerosol number concentration in the high aerosol case (10 × Control) is still noticeably higher after 2.5 days of simulations compared to the lower aerosol concentration cases, even though it is only the boundary conditions that control the changes in aerosol concentrations throughout the simulations. The higher aerosol concentrations in 10 × Control are especially noticeable at model levels below about 6 km in Figures 2a and 2b. Note that these are also the levels where most of the droplet formation occurs. At higher altitudes where variations in aerosol concentration are lower, droplet formation is less important.

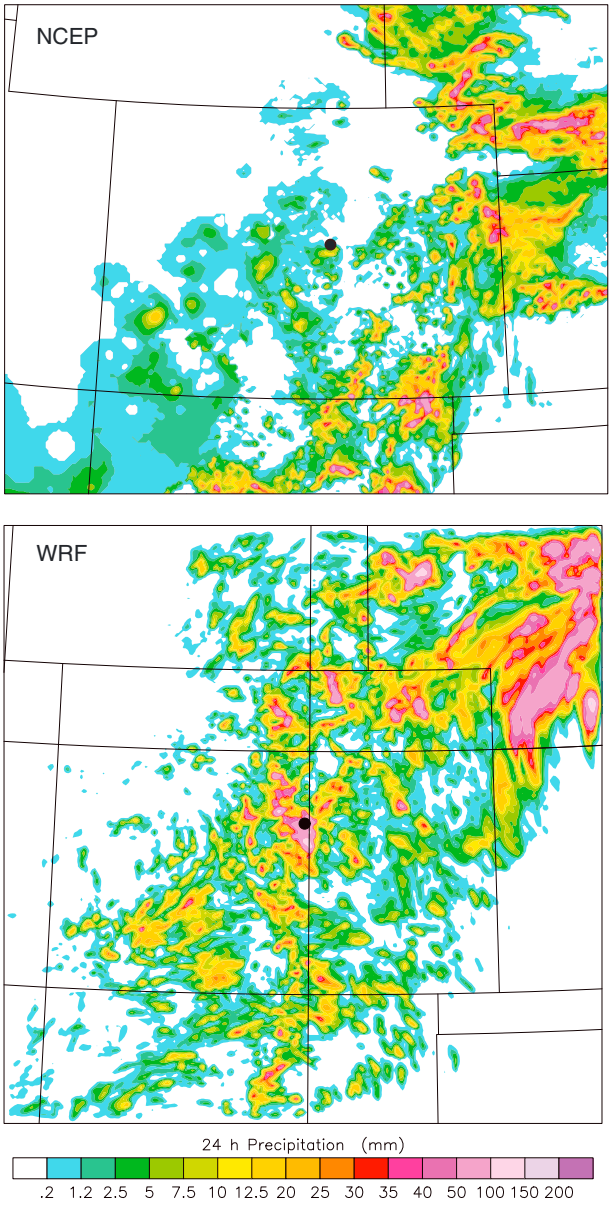

Figure 3. Twenty-four hour cumulative precipitation ending at 5 August, 12 UTC for (top) NCEP stage IV reanalysis and (bottom) model results. The black dot marks the MEF site.

Observations of CCN at $S = 0.56\%$ in August at the MEF site show an average concentration of about 600 cm^{-3} [*Levin et al.*, 2012], which is about what is seen in Figure 2c for the Control case.

Based on measurements at the Colorado Mountain Research Station (100 km northwest of MEF, see Figure 1), *Boy et al.* [2008] suggest that small particles (nucleation mode size) can both be formed locally, or be transported from upwind sources. *Cui et al.* [2014] found from a modeling study during BEACHON-RoMBAS that events of enhanced small particle number concentration and subsequently growth at MEF were associated with the transport of SO_2 from nearby pollution sources (typically Colorado Springs). At the time this work was conducted, the MOSAIC aerosol model did not yet account for new particle formation (NPF) of organic aerosols and growth of organics (secondary organic aerosols), which is one of the components that the BEACHON program studied. To account for NPF and growth in the model and study the importance of NPF on clouds and precipitation, we ran three additional sensitivity simulations: NPF23: NPF on 2 and 3 August; NPF234: NPF on 2, 3, and 4 August; and NPF34: NPF on 3 and 4 August.

For these NPF simulations, we have implemented an ad hoc mechanism that treats new particles as emissions of organics into the first modeled organics aerosol size bin. Since the smallest particle size in MOSAIC is 0.04 μm, we do not consider the initial new ultrafine particles. Instead, the emission of organic particles into the aerosol size bin is to represent the growth on newly formed or transported ultrafine particles. To reduce computational cost, these simulations were run with four size bins instead of the typical setup with eight size bins. Tests show that the precipitation did not change when reducing the amount of size bins (not shown here). In these cases, the smallest size bin includes particles with diameters from 0.04 to 0.16 μm in diameter. The new organic particles in the model are emitted into the surface layer with a rate of 0.5 $\mu g\, m^{-2}\, s^{-1}$ over areas of evergreen and needleleaf forest and savanna for a few hours in the afternoon (18 UTC–24 UTC, 12–18 MDT local time) for a set of modeling day combinations. The emission rate in the model is fairly high, as the highest emission rate of organic carbon aerosols over urban Denver is about 0.1 $\mu g\, m^{-2}\, s^{-1}$. The emission rate of 0.5 $\mu g\, m^{-2}\, s^{-1}$ was chosen since we do not account for gas to aerosol conversion, and such that in the NPF events, a few thousand new particles would be ingested into the first aerosol size bin. *Cui et al.* [2014] show that aerosol concentrations of sizes between 0.04 and 0.1 μm at the MEF site can range between ~4000 to 12000 cm^{-3} during new particle formation events. Here we are mostly interested in the sensitivity of clouds and precipitation from potential growth of new particles (represented by the particles ingested into the first size bin),

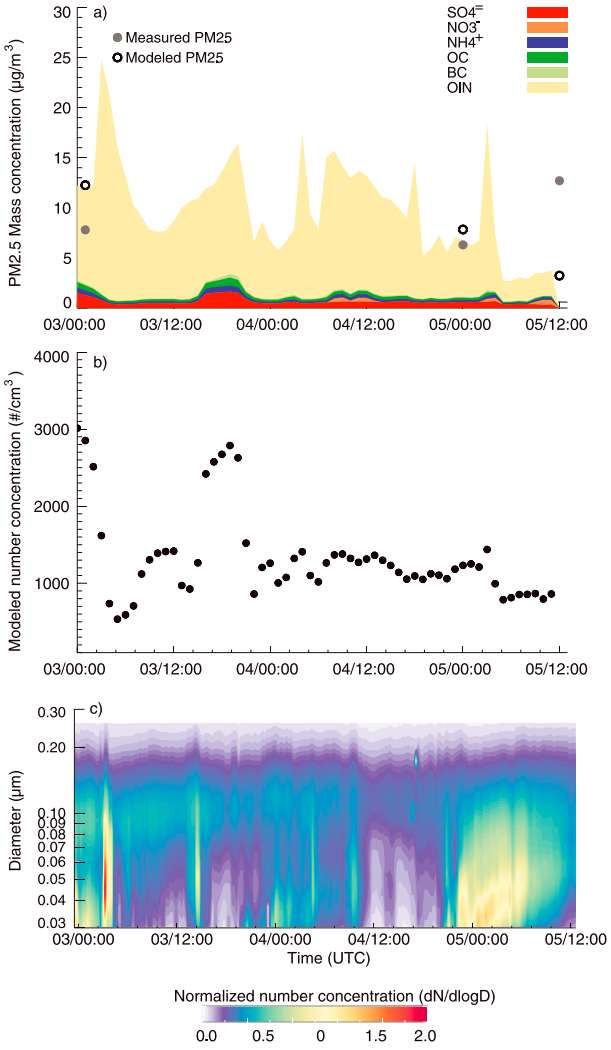

Figure 4. (a) Modeled $PM_{2.5}$ mass concentrations. The symbols show the 12 h average modeled and measured mass concentrations. (b) Modeled CN concentration for particles $>$ 0.04 μm. (c) Temporal evolution of the measured normalized CN size distribution ($dN/d\log D$). The time series is normalized such that the integral of $dN/d\log D$ is unity at 03:15 UTC on 3 August (location of maximum number concentration).

which might reach cloud level and act as CCN. Thus, for these experiments, we believe a simple representation of NPF and growth is sufficient. We do note that recent work has been conducted to include NPF of organic aerosols in MOSAIC [*Cui et al.*, 2014; *Matsui et al.*, 2011, 2014].

3. Measurements and Model Comparison

All simulations were run for 3 days, but we focus the aerosol-precipitation study mainly on the two last days (3 August, 12 UTC to 5 August, 12 UTC), when most of the precipitation in the model domain occurred. A fairly stagnant cold front was located just north of Colorado during most of the modeling time period. Precipitation from convective, mixed-phased clouds occurred during both afternoons. Figure 3 shows the 24 h Control case-modeled precipitation and the National Centers for Environmental Prediction (NCEP) stage IV reanalysis, for 5 August. As shown, the overall precipitation pattern compares reasonably well between model and observations for this case. However, the precipitation in the model is shifted more toward the west and is heavier over the mountainous region of Colorado compared to the NCEP IV reanalysis. This modeled precipitation came from several individual small convective clouds developing over the mountain region. Further, the WRF model overestimates the precipitation in the northeast corner of the domain. This overestimation in the model could be due to boundary conditions. Further analyses presented here omit the region close to the model boundaries (Figure 1). Also, studies show that the Lin microphysics scheme, which is used here, has a tendency to produce more graupel compared to other microphysical schemes [e.g., *Liu et al.,* 2011; *Segele et al.,* 2013], and *Liu et al.* [2011] showed that this high amount of graupel produced too much precipitation compared to observations in orographic wintertime precipitation systems.

Figure 4a shows the modeled $PM_{2.5}$ mass concentrations and the relative contributions from the different chemical species. Also shown are $PM_{2.5}$ measurements taken at the MEF site, which give the 12 h average $PM_{2.5}$ mass concentrations. We have only three 12 h measurements during the modeling period; for the first two points, the model is slightly higher than the measured values, which may be a result of using the 2005 EPA emissions inventory that has higher $PM_{2.5}$ emissions than their 2008 inventory. Yet after 5 August, 03 UTC, the model fails to capture the increase seen in the mass concentration. Modeled OIN contributes most to the total modeled $PM_{2.5}$ mass loading, while sulfate contributes most of the nonrefractive particles.

Although we do not have number concentration measurements to evaluate the modeled number concentration (section 2.2), we believe that the modeled particle number concentration (Figure 4b) from our control run

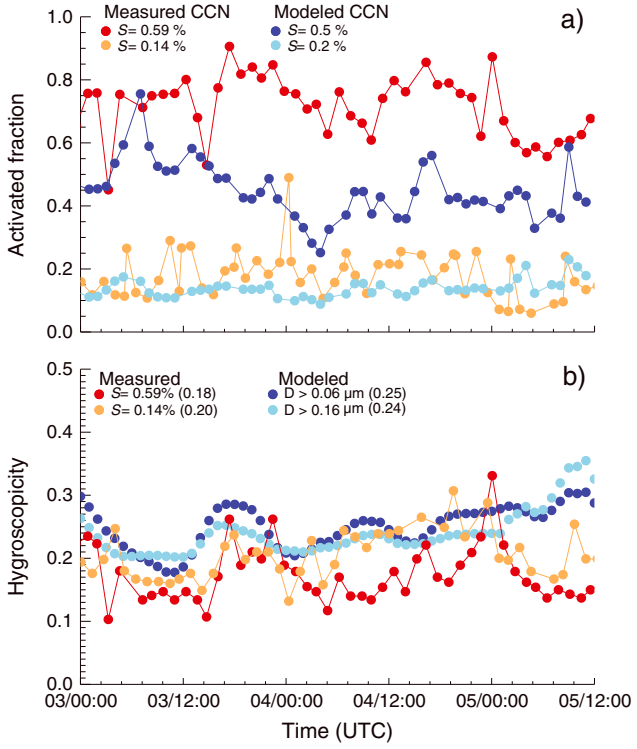

Figure 5. (a) Activated fraction ($CCN_{0.04}/CN_{0.04}$). Modeled (from the lowest model level, blue circles) at 0.5 and 0.2% supersaturation and measured (red and orange circles) at 0.59 and 0.14% supersaturation. (b) Calculated hygroscopicity, κ_{avg}. For the measurements, κ_{avg} is estimated at the different supersaturations. For the model, κ_{avg} is calculated for particles greater than a certain size, comparable with D50 at the measured supersaturations. Average hygroscopicity values are included in parenthesis.

underestimates the observed number concentration based on ancillary evidence. First, *Cui et al.* [2014] showed that WRF-Chem predictions, using the MOSAIC aerosol module, underestimated CN concentrations during the BEACHON-RoMBAS experiment in July–August 2011. Second, the small particle event seen in the temporal variation of the MEF measured normalized aerosol size distribution (Figure 4c, ~00 UTC on 5 August) was not predicted by the WRF-Chem model (Figure 4b). In these small particle events, the particle number concentrations can increase up to about 10,000 cm^{-3} [*Cui et al.*, 2014] for particles between 0.04 and 0.1 µm.

CCN concentrations are calculated in WRF-Chem at supersaturations S of 0.02, 0.05, 0.1, 0.2, 0.5, and 1%, while measurement supersaturations were ~0.14, 0.41, 0.59, and 0.78%. Assuming that the composition of modeled aerosols is comparable with the measured aerosol population and the modeled size distribution shape is reasonable, the activated fraction (CCN number concentration/CN number concentration) should be comparable between model and measurements. However, Figure 5a shows that the modeled activated fraction of particles > 0.04 µm ($CCN_{0.04}/CN_{0.04}$) underestimates the measurement for the higher supersaturations (not shown is that even the measured fraction at $S = 0.41\%$ is higher than modeled fraction at $S = 0.5\%$). At the lower supersaturations (sensitive to larger particles), the modeled and measured activated fractions compare better. We will analyze the composition and size distribution to assess possible causes for this discrepancy.

An indirect method to estimate the composition of the aerosols is to determine the hygroscopicity (κ) of the aerosols since aerosols have various hygroscopicity depending on their composition. The average hygroscopicity from model results is determined with the mixing rule described by *Petters and Kreidenweis* [2007]. For each modeled size bin, an average κ_{bin} is determined by using the following:

$$\kappa_{bin} = \sum\nolimits_i \varepsilon_i \kappa_i, \quad (1)$$

where ε_i is the volume fraction of individual species compared to the total mass of all the species in that size bin. The average hygroscopicity for the entire aerosol population (κ_{avg}) is then found by normalizing over the number concentration in each bin to obtain the number weighted average. In WRF-Chem, $\kappa = 0.5$ for SO_4^{2-}, NO_3^-, and NH_4^+, $\kappa = 0.14$ for OIN and OC, and $\kappa = 1E^{-6}$ for BC. Figure 5b shows a time series of κ_{avg} as determined from the model and measurements. The measured κ_{avg} values are shown for $S = 0.14\%$ and $S = 0.59\%$. The modeled κ_{avg} is superimposed for the size for which 50% of the measured aerosols are activated (D50) at $S = 0.14\%$ (D50 ~ 0.16 µm) and at $S = 0.59\%$ (D50 ~ 0.06 µm). The modeled and measured κ_{avg} values compare reasonably well during the first analysis day, with the modeled κ_{avg} being slightly higher than that measured. We note that the κ value for OIN used in WRF-Chem is higher than what measurements suggest for dust [*Koehler et al.*, 2007], who found that $\kappa \approx 0.04$. By using $\kappa = 0.04$ for OIN instead, the modeled average hygroscopicity decreases by about 0.02. On the second and third day, the modeled κ_{avg} tends to be significantly higher than κ_{avg} derived from measurements, particularly on the last modeling day when the

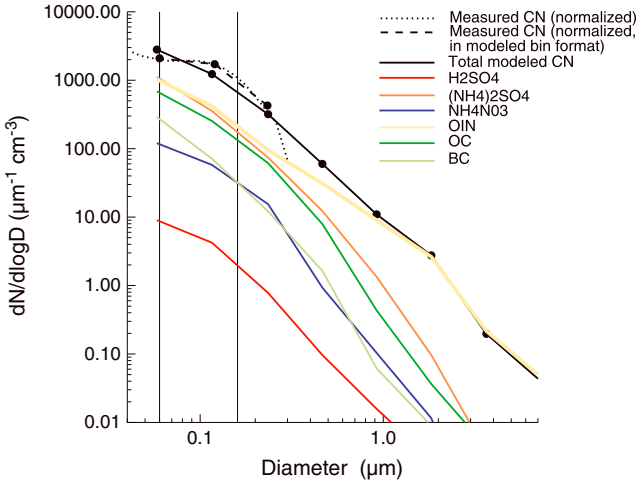

Figure 6. Modeled and measured normalized temporal averaged size distribution. Dots indicate the midpoint of the modeled size bins. Since the absolute number concentration from measurements is not available, the measured size distribution is normalized to match total number concentration in the model over the first three size bins (these are the bins where the model and measurements overlap). The dashed line shows the normalized measured number concentration, but the size bins are combined to match the modeled size bins. Vertical lines indicate the activation size (D50) at $S \sim 0.14\%$ and $S \sim 0.59\%$. Also included are the modeled chemical-specific distributions, assuming externally mixed aerosols.

measured κ_{avg} is about 0.15 while the modeled κ_{avg} is closer to 0.3. If the differences between the model and the measured activated fractions could be explained only by differences in hygroscopicity, the modeled activated fraction in Figure 5a would be higher than the measurements since the modeled κ_{avg} values are higher. However, this is not the case.

The cause of the discrepancy between the modeled and measured activated fraction can potentially be explained by comparing the modeled and measured total size distribution (Figure 6). Again, absolute number concentration from measurements was not available. In Figure 6 the measured size distribution is normalized to match total number concentration in the model over the first three size bins (these are the bins where the model and measurements overlap). The figure shows that the modeled shape of the size distribution deviates from the measurement. The overall effect is that the modeled size distribution has a higher fraction of smaller particles that do not activate compared to measurements (Figure 5a). Consequently, the lower activated fraction in the model may be explained by the failure to accurately reproduce the size distribution.

According to the average hygroscopicity calculations (which is number weighted) the model contains aerosols that are more hygroscopic than those measured. This could be due to underestimation of organic carbon fraction in the smaller sizes, as also found in *Cui et al.* [2014]. In Figure 6, as an illustration, the aerosols are divided into individual species, assuming external mixing. Clearly, the fraction of ammonium sulfate $(NH_4)_2SO_4$ at the smaller sizes is higher than the fraction of organics, contrary to the findings of *Levin et al.* [2012, 2014]. *Levin et al.* [2014] determined from a yearlong study of CN and CCN at the MEF site that organic mass fraction of nonrefractive particles less than 0.35 μm was 70 to 80% of the aerosol composition. In the model, the organic mass fraction of the nonrefractive particles is about 30%. Inclusion of more organics via new particle formation and subsequent growth of secondary organic aerosols in the model version used here would reduce the hygroscopicity value.

The higher modeled hygroscopicity could also be in part due to deficient modeling of OIN. In the modeled size distributions, the OIN category represents a large fraction of the aerosol number concentration at all sizes (Figure 6) and is comparable with the contribution from ammonium sulfate at the smallest sizes. Thus, a relatively high OIN fraction, combined with the previously mentioned high κ value used for OIN, will increase the hygroscopicity slightly.

The missing increase in modeled aerosol concentrations, as seen in the observations on 5 August (Figure 4c) may, in addition to lack of new particle formation and growth of organics, also be impacted by the modeled wet deposition of the aerosols in the model. Measurements at the MEF site did not detect any precipitation during the study period, while the modeled precipitation was about 50 mm. Thus, a portion of the aerosols was washed out in the model (not shown), which did not happen at the site in reality. This event was the only major modeled precipitation event at the MEF site.

Finally, for comparison, we also calculated the overall estimated hygroscopicity values from the 10 × Control and 0.2 × Control simulations. The 10 × Control hygroscopicity ($\kappa_{avg} = 0.39$ for $D > 0.06$ μm and $\kappa_{avg} = 0.41$ for $D > 0.16$ μm) is higher than the Control simulation, while the 0.2 × Control hygroscopicity ($\kappa_{avg} = 0.21$ for

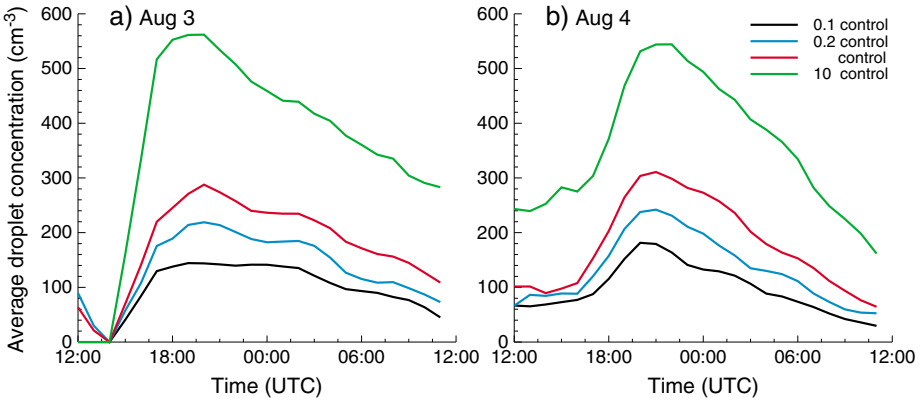

Figure 7. Average droplet concentrations at model level 9 (~1700 m above ground), (a) 3 August and (b) August 4.

$D > 0.06$ μm and $\kappa_{avg} = 0.19$ for $D > 0.16$ μm) is lower. The best comparison between the measured ($\kappa_{avg} = 0.18$ for $S = 0.5\%$ and $\kappa_{avg} = 0.20$ for $S = 0.21\%$) and modeled hygroscopicity is when the sulfates and ammonium concentrations are decreased by a factor of 0.2 from the control run.

Although the model does not predict the observed composition exactly, the model sensitivity to variations in aerosol concentrations and those effects on clouds and precipitation can still be successfully explored. For example, a change in κ_{avg} from 0.2 to 0.4 is not expected to have much impact on clouds and precipitation [*Dusek et al.*, 2006; *Ward et al.*, 2010; *Reutter et al.,* 2009]. Composition has less of an effect on clouds than aerosol number concentration and size, especially for convective clouds with high updrafts and supersaturations. In our model simulation, domain-wide κ_{avg} values usually were between 0.15 and 0.30 in the Control simulation with a few locations with a minimum of κ_{avg} ~0.1 and a maximum of κ_{avg} ~0.5.

4. Aerosol and Cloud Interaction Sensitivity Results

4.1. Aerosols and Precipitation

To assess the aerosol effect on clouds and precipitation in the modeled simulations, we present results mainly from the last two modeling days (from 3 August, 12 UTC (6 MDT), to 5 August, 12 UTC (6 MDT)), since these are the days with the most precipitation.

Figure 7 shows the average droplet number concentration at cloud base (model level 9 (~1700 m above ground), from all grid points containing droplet concentrations greater than 5 cm^{-3}) throughout the second and third modeling days. There is a clear difference in the number concentration between the different simulation runs, from cleaner (0.1 × Control) to the more polluted (10 × Control) case, with the polluted case having about 3 times more droplets than the cleanest case (0.1 × Control). There is also a nonlinearity in the results, with a larger difference between the Control and 10 × Control compared to the difference between the 0.1 × Control and Control simulations.

Figure 8 shows the average domain-wide hourly and cumulative precipitation for the four different simulations. Note that with domain wide, we mean the analyzed domain, and the regions near the boundaries are not included (see section 2). The precipitation systems start at the same time for all simulations on both days, and there is little delay in the onset of precipitation between the different cases, even though these are the second and third simulation days. This result suggests that large-scale dynamical forcing controls the timing of the precipitation systems, and the aerosols affecting cloud microphysics therefore do not have a considerable effect on the large-scale dynamics. However, we only saved hourly model outputs, and differences at smaller time scales are not considered. *Cui et al.* [2011] and *Teller and Levin* [2006] report a general delay (on the order of 10 to 20 min) in the onset of precipitation with increased aerosol loading due to slower formation of graupel (small droplets freeze at a slower rate than larger droplets). The 2 days show about the same response to changes in aerosol. For the case with 10 × Control, the precipitation decreases ~8% on the second modeling day, and ~5% decrease on the third modeling day. For the cases where we decreased the aerosol concentrations (0.1 × Control and 0.2 × Control), both cases show a small increase in precipitation over the entire domain on both days of ~5%.

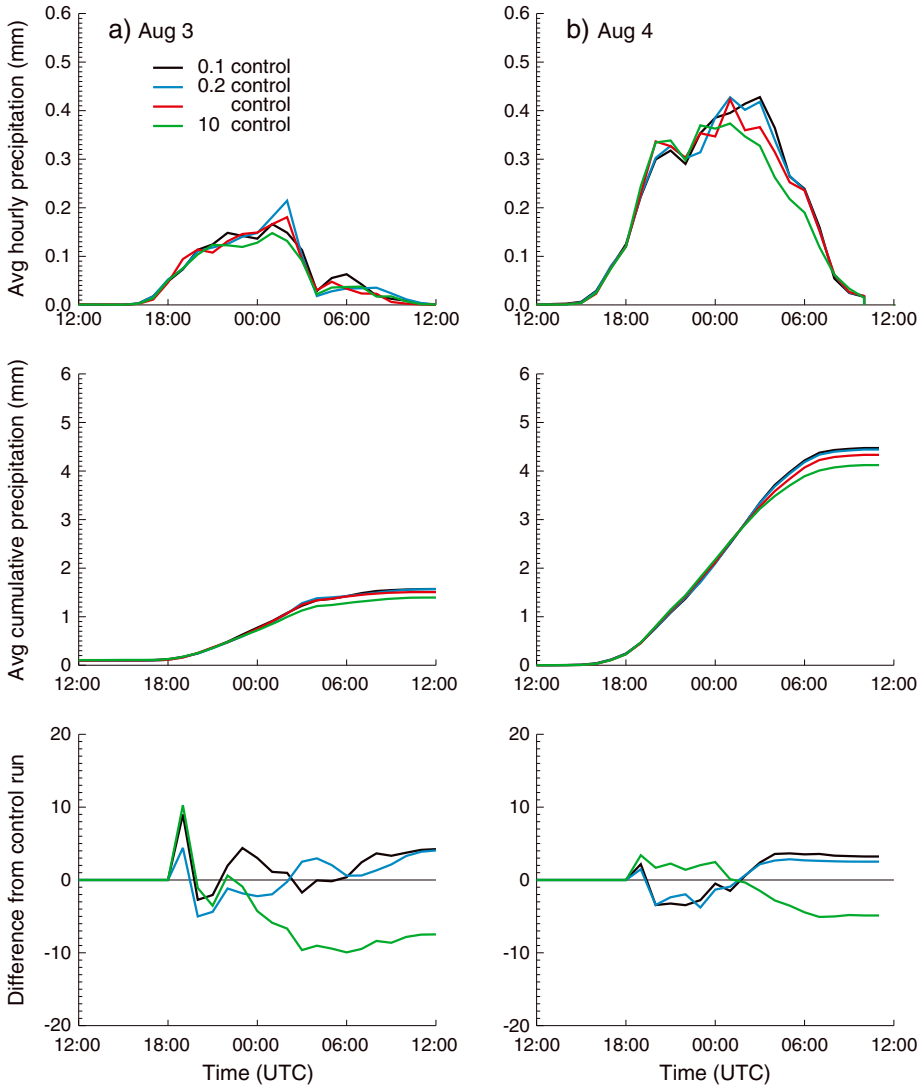

Figure 8. Average domain-wide (top) hourly and (middle) cumulative precipitation for (a) 3 August and (b) 4 August. (bottom) The percent difference of the cumulative precipitation from the Control simulation.

Comparison of these results with other studies shows some similarities. For example, in Table 4 in the review paper by *Tao et al.* [2012], the results from several convective aerosol-cloud-precipitation studies are summarized. The percent change in precipitation ($dP = 100 \times (P_{dirty} - P_{clean}) / P_{clean}$) for a given change in CCN concentration ranges from −250% to +700%, with most of the results being less than ±100%. The change in CCN concentration from low to high values (dN_{CCN}) varies among the different studies along with the starting CCN number concentration (N_{CCN}), and some of the variation in the dP originates from variations in dN_{CCN} between the different studies. We therefore include the percent change (Figure 9a) and the precipitation susceptibility dP/dN_{CCN} as a function of initial CCN (or droplet) number concentration (Figure 9b). We do not use the definition by *Sorooshian et al.* [2009], where the precipitation susceptibility is defined by $d\ln P/d\ln N_d$, since here we only know dP in percent from *Tao et al.* [2012]. The results from Tao et al. are shown as grey-shaded circles, where different grey shades represent different intervals of precipitation changes in percent. The largest precipitation susceptibility to changes in CCN number concentration is for initial low values of CCN. For the cases with initial $N_{CCN} > 500\ cm^{-3}$, the change in precipitation to change in CCN is fairly low. This conclusion is also supported by other studies [e.g., *Wang*, 2005].

The susceptibility in Figure 9b is calculated for changes from the lowest initial droplet concentration to the highest droplet concentration for all cases, while the dP shown in Figure 8 is the difference from the control

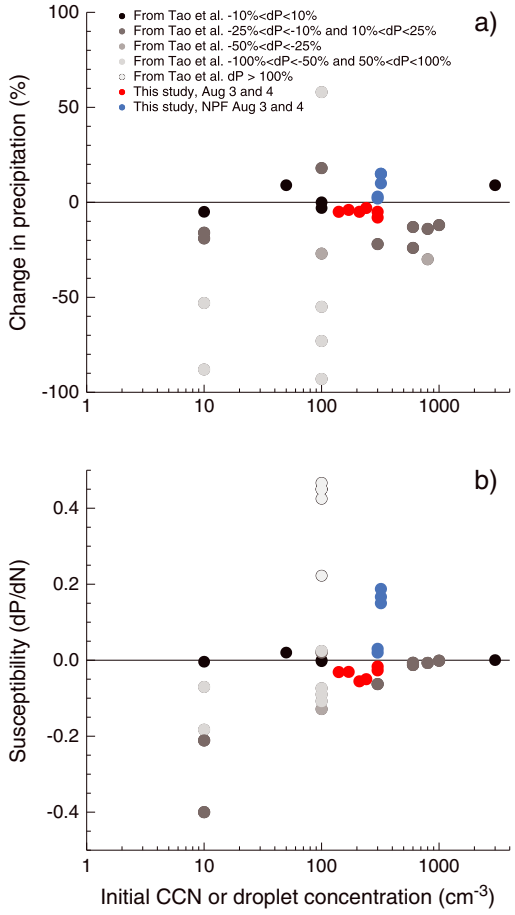

Figure 9. (a) Precipitation changes (from clean to polluted cases) from studies listed in Table 4 in *Tao et al.* [2012] (gray scale circles). Colored circles are results from this study. On the *x* axis is the CCN or droplet number concentration in the clean case. (b) Precipitation susceptibility to changes in CCN or droplet concentration.

simulation: ($dP = 100 \times (P_{sensitivty} - P_{control})/P_{control}$). For the three different sensitivity cases for the two modeled days the susceptibility are Day2: 0.1 × Control: −0.03, 0.2 × Control: −0.06 and 10 × Control: −0.03; Day3: 0.1 × Control: −0.03, 0.2 × Control: −0.05, and 10 × Control:−0.02. The susceptibility values are shown in Figure 9b as red circles. The susceptibility in this study are comparable with the examples from Tao et al.

The examples from Tao et al. in Figure 9 are mostly from 2-D models for individual events and for short time scales (a few hours to maximum 3 days). A few recent WRF-Chem studies using the same microphysical scheme as our study have been published. For example, *Chapman et al.* [2009] report a 31% increase in precipitation with a decrease in aerosol emission such that aerosol optical depth decreases from 0.46 to 0.38 for a frontal passage case over western Pennsylvania in August (no droplet concentration information was included in this paper, so we cannot determine the susceptibility). *Zhao et al.* [2012] also reported a 30% decrease in precipitation when a sulfate plume from long-range transport was ingested at the bottom of the cloud. The initial CCN concentration at 0.4% supersaturation was ~160 cm^{-3} for the base case while the plume increased the droplet concentration by ~120 cm^{-3}. Both of these studies report a larger response in clouds to increases in aerosol concentrations than what we found. However, these two studies also included aerosol direct effects for which the aerosols have the potential to change the temperature gradient and stability due to the absorption and scattering of the aerosols. The direct effect is not included in our study.

In previous studies, it is found that the state of the environment has an impact on the sign of the precipitation change. *Rosenfeld et al.* [2008] and *Khain et al.* [2008] found that precipitation amount often increases with an increase in aerosol loading in humid environments. In the case simulated here, the relative humidity is about 60% at the first model level, which can be characterized as a drier environment. Thus, the decrease in precipitation with increasing aerosols found in most of the cases here is in agreement with *Rosenfeld et al.* [2008] and *Khain et al.* [2008]. *Rosenfeld et al.* [2008] (and references within) also state that the temperature at cloud base should be warmer than ~15°C for aerosols to cause convective invigoration, and from there increase the precipitation. The temperature at cloud base in our simulations are close to 0°C over the mountains and close to 5°C over the Plains; thus, the temperature in our simulations are much lower than for where increased aerosol loading could increase precipitation according to *Rosenfeld et al.* [2008]. Further, *Fan et al.* [2009] found that in environments with low wind shear, increases in aerosol loading will lead to an increase in precipitation. This is also supported by the study of *Lebo and Morrison* [2014]. Here the wind shear (between ground and about 6 km above sea level) in the southern part of the domain is between 2 to 7 m/s (low wind shear), while the wind shear in the northeastern part of the domain is between 10 and 17 m/s (strong wind shear, according to *Fan et al.* [2009, Table 1]). Thus, we have both low and high wind shear in our domain and could expect some mixed precipitation responses to aerosol changes. Finally, *Lee et al.* [2008] found that regions with high wind shear and high CAPE, along with high aerosol loading would lead to increases in precipitation. This is also supported by the results of *Ntelekos et al.* [2009]. We investigated if there were a difference in precipitation response in the southern (low wind shear) versus northern part

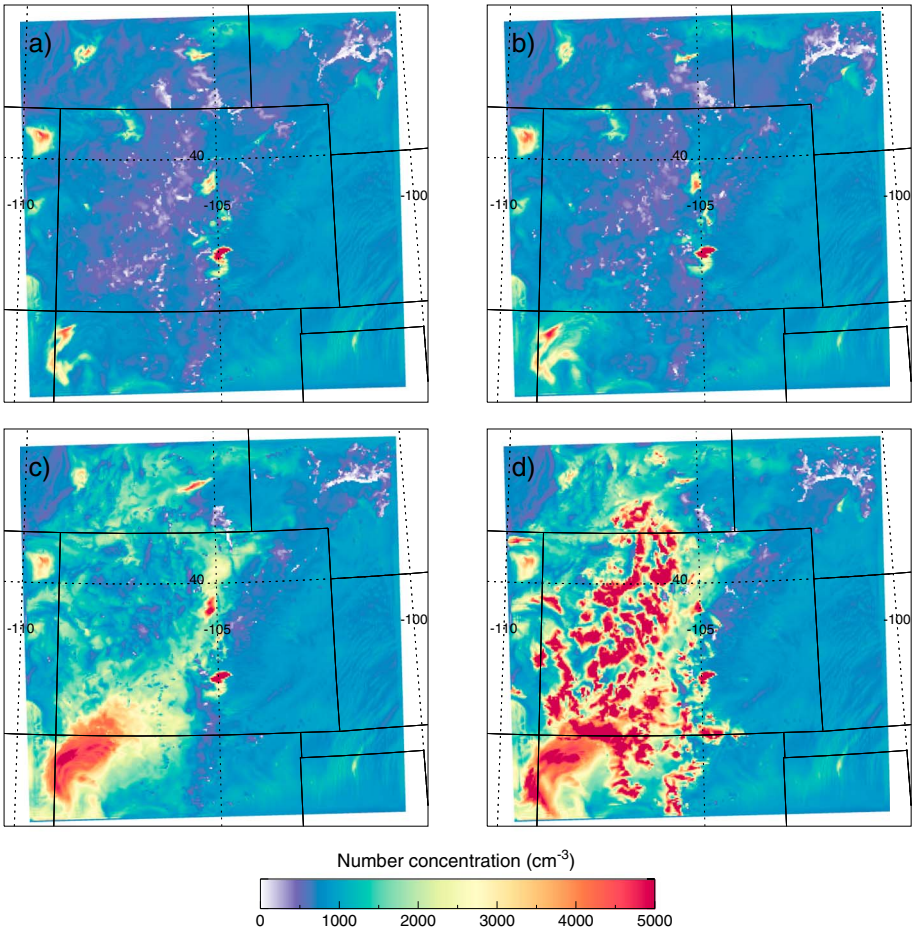

Figure 10. Modeled aerosol concentrations in size bin 1 (0.04–0.115 μm) at model level 9 (~1700 m above ground, cloud forming height) on 4 August 21 UTC. Cases shown are (a) control case (no NPF), (b) NPF on 2 August only, (c) NPF on 2 and 3 August (NPF23), and (d) NPF on all days (NPF234).

(high wind shear and small regions of higher CAPE) of the model domain but did not find a clear difference in regional response to increases in aerosols. For example, the 10 × Control case always had decreasing precipitation in all regions of the model domain. Thus, we find that the environment in the simulations conducted here did not support precipitation enhancement.

In summary, our simulations show when aerosol concentrations are increased that domain-wide precipitation decreased by 10% or less. These results are in accord with previous findings, especially those for less humid conditions. We did not find a dependence of precipitation amount on the vertical wind shear and CAPE.

4.2. NPF and Precipitation

In addition to the sensitivity tests described above, where aerosol mass was increased or decreased throughout the entire domain, we ran three sensitivity studies to explore the effect of the formation of new organic aerosols on precipitation (NPF23, NPF234, and NPF34, see section 3). Because organic aerosol emission occurred during the afternoon in the cases here, we show the spatially varying aerosol concentration in the smallest aerosol bin at 21 UTC (3 h after the emissions start, at model level 9, close to the cloud base) in Figure 10. The increased aerosol concentrations from NPF are located over the Rocky Mountains, especially in the southwest part of the domain. Figure 11 shows the hygroscopicity for the NPF234 case over the MEF site. At the end of the NPF periods (00 UTC), the modeled hygroscopicity compares better with the measurements than the control run (see Figure 6). This is best seen at the higher supersaturations (which allows for activation of the smaller new organic particles), where κ_{avg} is decreased by about 0.05 to 0.2 when the NPF in included.

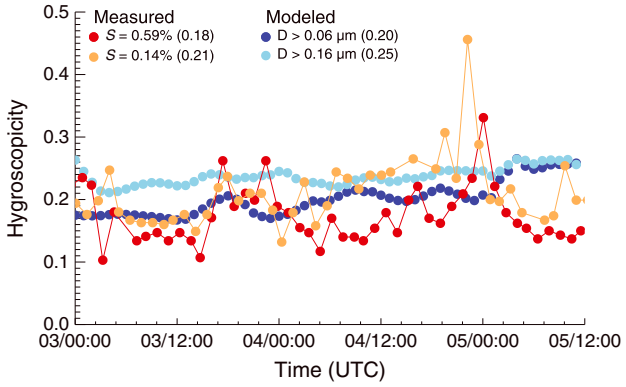

Figure 11. Same as Figure 5b but for the NPF234 case.

Figure 12 shows the average droplet concentration at ~1700 m (model level 9) for the control case (black line), along with the three NPF cases for 3 and 4 August (second and third modeling day). There is an increase of droplet concentration with increasing NPF. The overall change in droplet concentration is smaller than that found in the simulations described in the previous section, especially on 4 August. However, when considering changes in precipitation, we see a general response different from the results with no NPF considered. Figure 13 shows the domain-wide hourly and cumulative precipitation from the NPF cases along with percent changes in cumulative precipitation from the control (no NPF) case. When considering precipitation changes on 3 August, the increase in aerosols results in an increase in precipitation, but only by about 3%. This precipitation increase is also seen for 4 August, and the increase is as much as 20%. Further, these results are opposite from the results described in section 4.1. The susceptibility for this case is also shown in Figure 9 (dark blue circles). For the 3 August case (NPF23) the susceptibility is +0.02, while for 4 August (NPF234), the susceptibility is between 0.1 and 0.2 and is much higher than most of the other studies shown in Figure 9, specifically for the initial CCN concentration of 300 cm^{-3}.

The main precipitation difference in the NPF simulations compared to the no NPF case on 4 August starts around 18 UTC, when a system in the northeastern part of the domain develops in the NPF simulations (not shown here). This development is not seen in the previous simulations (0.1 × Control, 0.2 × Control, Control, and 10 × Control), for which we determined that the environment is most likely not conducive for precipitation enhancement. However, *Morrison and Grabowski* [2013] found that when imposing perturbations (mimicking the aerosol invigoration effect) in clouds across an entire modeling domain, any perturbed convection went back to the unperturbed state after about 24 h due to feedbacks with larger-scale environments. Yet if the perturbations were only applied to a part of the domain, gravity waves from the perturbed region dispersed buoyancy anomalies to the rest of the domain, and convective invigoration was seen for the entire modeling time period, which was about 7 days in their study. In our NPF simulations, only some areas within our domain are affected by increased aerosol concentrations (Figure 10). It is possible then that the increase in precipitation in the NPF cases results from the conditions described by *Morrison and Grabowski* [2013].

4.3. Uncertainties and Limitations

The findings from our model simulations show small changes in domain-wide precipitation (~5%) when a uniform change to the model initial and boundary conditions was imposed, while simulations with localized

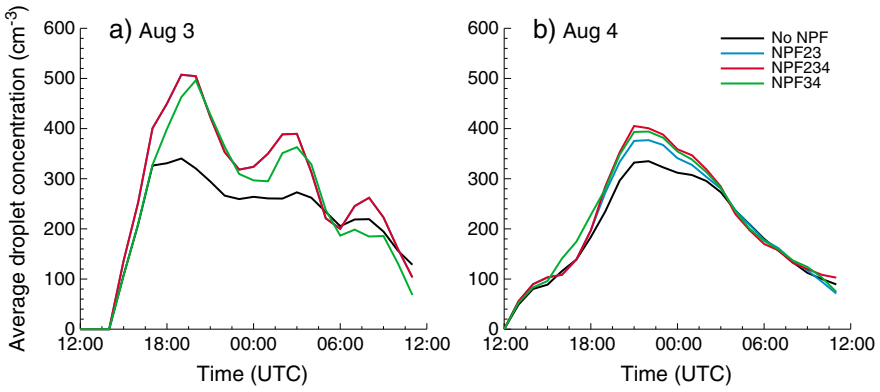

Figure 12. Average droplet concentrations for the NPF cases at model level 9 (~1700 m above ground); (a) 3 August and (b) 4 August.

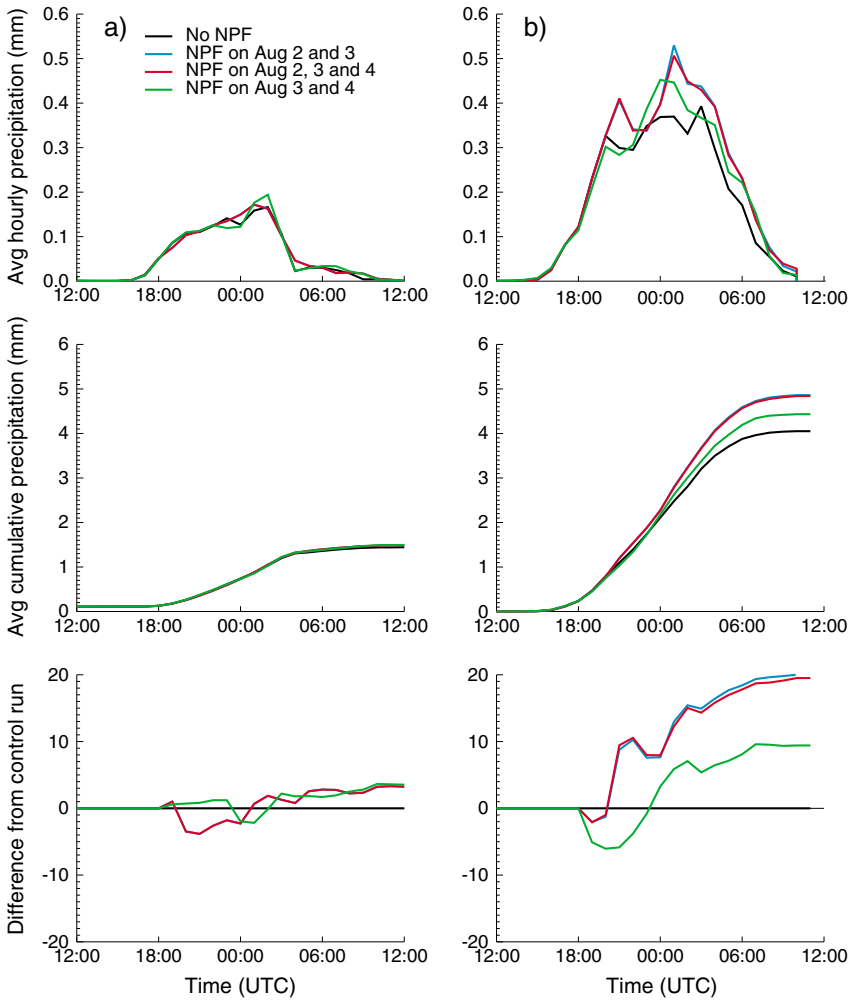

Figure 13. Same as Figure 11 but for the NPF sensitivity cases. Note that on 3 August, NPF23 and NPF234 is exactly the same; thus, only the red curve is shown in Figure 13a.

increases in organic aerosol emissions produced increased precipitation. These results depend on the capabilities of the model parameterizations and how much these parameterizations are realistic. Here we discuss uncertainties and limitations of our simulations.

First, at the time of conducting this study, the latest version of the EPA National Emissions Inventory was the 2005 version. The newer, 2008 version shows that emissions of compounds such as SO_2 and NO_x have decreased, especially in New Mexico where the decrease was about 60%. In Colorado, the decrease was only about 6%. The emission of $PM_{2.5}$, which is placed into the OIN category also decreased by up to 80%, both in Colorado and New Mexico. Thus, model predictions of $PM_{2.5}$ are somewhat higher than observations. However, these changes in SO_2 and $PM_{2.5}$ emissions are less than those that were imposed by our sensitivity simulations that examined aerosol microphysical effects on precipitation. Thus, we do not expect the choice of emissions inventory to affect the conclusions of this paper.

We implemented a simple ad hoc approach accounting for new organic aerosol particle formation. We allow for additional new particles in the smallest size bin during the entire afternoon, over a relatively large area, irrespective of meteorological conditions such as temperature, humidity, precipitation, and wind direction (which can bring necessary compounds from polluted sites that can trigger the new particle formation). Thus, our estimations of new particles are likely extreme but nevertheless important for understanding the sensitivity of clouds and precipitation to variations in aerosol concentration from new particle formation.

A shortcoming of the cloud activation scheme used here is that it does not allow for secondary formation of cloud droplets in deep convective clouds. Because convective updrafts are large, supersaturation and therefore cloud drop activation from aerosols can be experienced above cloud base. Investigations into the importance of this process should be done in future modeling studies and confirmed with field observations. Further, the *Lin et al.* [1983] cloud microphysical scheme used here is only a one-moment bulk scheme, (except for cloud droplet formation), but snow, graupel, and ice number concentration (and size) can be affected by changes in the amount of droplets produced. Newer versions of WRF-Chem do include the ability to assess aerosol-cloud interactions using a double moment cloud physics scheme.

To evaluate the model, the only measurements available were taken at a surface site. However, the aerosol concentrations near cloud base are important for what actually goes into the cloud. While the surface measurements give a picture of some model biases that can also affect aerosols at cloud formation heights, such as biases in concentrations and composition, aircraft observations would be much better to have. Field studies (e.g., Green Ocean Amazon) that include aircraft observations should be encouraged for semiarid locations.

5. Summary and Conclusions

We present a WRF-Chem modeling study, for which we compared with measured aerosol properties at the Manitou Experimental Forest (MEF) site and performed sensitivity studies to investigate the impacts of changing aerosol concentrations on precipitation during the North American monsoon season in Colorado in August. Many previous aerosol-cloud interaction modeling studies have only been idealized, not allowing for interactions with the dynamics as well as only been set up for two dimensions. This model study enables the study of aerosol-cloud-precipitation interactions with dynamical feedback and the inclusion of realistic meteorological input and aerosol processes allowing for spatial and temporal variations of aerosols.

When compared with measurements from the MEF site, the modeled average hygroscopicity factor (κ_{avg}) in the control simulation is generally higher than the ones determined from measurements. While measurements indicate that the organic fraction of the nonrefractive species at the MEF site is about 70–80% [*Levin et al.*, 2014], the model only produced an organic fraction of about 30%. This underestimation of the organic fraction of the nonrefractive species is most likely caused by the lack of new, organic aerosol production (new particle formation) and growth of secondary organic aerosols in version 3.1.1 of the WRF-Chem model. The higher κ_{avg} values from the model indicate that the model contained a higher fraction of hygroscopic aerosols (typically ammonium sulfates) than what is actually observed. When the simulations included an ad hoc new particle formation mechanism, assumed to be organics, the estimated hygroscopicity of aerosols at the MEF site is improved slightly. Thus, the lack of new particle formation and the condensation and growth of organics in the aerosol module used here (MOSAIC) could have caused the CN and CCN concentrations in the control simulations to be lower than actual concentrations.

The aerosol-cloud-precipitation study was of a 3 day convective precipitation system during the North American monsoon season, with modeled convective precipitation specifically over the Colorado Rocky Mountain region as well as precipitation in the plains over northeast Colorado and southwest Nebraska. Several modeling studies have suggested that increases in aerosols can lead to increases in precipitation in convective systems under certain environmental conditions. For the cases here where aerosol concentrations are changed uniformly over the domain ($0.1\times$Control, $0.2\times$Control, and $10\times$Control), the domain-wide cumulative precipitation shows a pattern of decreasing precipitation with increasing aerosol concentration. When considering the environmental conditions in our case, (relative humidity, temperature at cloud base, wind shear, and CAPE), we find that the case presented here does not have any of the environmental conditions required for precipitation enhancement with increasing aerosol loading.

The precipitation susceptibility was calculated to assess the change in precipitation when aerosol number concentration is changed. Our results, for the cases where aerosol concentration is changed uniformly over the domain, have susceptibilities as low as -0.05. The results presented here (e.g., Figure 9) are in the range of those presented in other studies.

An ad hoc process to account for new particle formation in the model was included in a second set of model simulations. This was accomplished by increasing the emissions of organics (to mimic NPF and subsequent growth of aerosols) over areas of evergreen and needleleaf forest and savanna for 6 h in the local afternoons.

The emissions of organic aerosols were inserted into the first aerosol size bin at the model surface layer. By doing this, the increase in aerosols was not distributed evenly in the model domain. The ad hoc NPF led to an increase in droplet concentration, but not as high as in the 10 × Control case. However, all NPF cases resulted in both droplet concentrations and precipitation amounts increasing. This is opposite of what was seen in the cases where aerosol concentrations were changed uniformly over the domain. We speculate that the different response in precipitation between the NPF cases and the uniform aerosol change cases can be due to the dynamical response of localized perturbations, similar to the processes described by *Morrison and Grabowski* [2013]. However, additional modeling studies, focused on this hypothesis, need to be conducted to verify this assumption.

Although these simulations allow for linking aerosol-cloud interactions with dynamics, they did not include aerosol impacts on radiation (aerosol direct effect), and thus, the full dynamical interactions were not included. In the future, we suggest the use of more realistic new particle formation and secondary organic aerosol models, along with more advanced cloud microphysical schemes.

Acknowledgments

NCAR is sponsored by the National Science Foundation. The CN and CCN data used in this study were obtained through the collaborative use of instruments funded by the NSF Major Research Instrumentation, Atmospheric Chemistry, and Physical and Dynamic Meteorology programs through grant 0521643 awarded to Colorado State University. The gathering of the CN and CCN data was supported by the NSF grant ATM0611936 and the NASA grant NNG06GF00G. We acknowledge Kip Carrico for support with making use of the CSU Mobile Laboratory, which is supported by the National Park Service (NPS). We also thank Kelly Barsanti, Mike Hannigan, and Jim Smith for the gathering and analysis of the $PM_{2.5}$ data. The data used to produce the figures are available by contacting the first author.

References

Abdul-Razzak, H., and S. J. Ghan (2002), A parameterization of aerosol activation, 3: Sectional representation, *J. Geophys. Res.*, *107*(D3), 4026, doi:10.1029/2001JD000483.

Albrecht, B. (1989), Aerosols, cloud microphysics, and fractional cloudiness, *Science*, *245*, 1227–1230.

Andreae, M. O., D. Rosenfeld, P. Artaxo, A. A. Costa, G. P. Frank, K. M. Longo, and M. A. F. Silva-Dias (2004), Smoking rain clouds over the Amazon, *Science*, *303*, 1337–1342, doi:10.1126/science.1092779.

Boy, M., et al. (2008), New particle formation in the Front Range of the Colorado Rocky Mountains, *Atmos. Chem. Phys.*, *8*, 1577–1590, doi:10.5194/acp-8-1577-2008.

Chapman, E. G., W. I. Gustafson, R. C. Easter, B. C. Barnard, S. J. Ghan, M. S. Pekour, and J. D. Fast (2009), Coupling aerosol-cloud-radiative processes in the WRF-Chem model: Investigating the radiative impact of elevated point sources, *Atmos. Chem. Phys.*, *9*, 945–964.

Chen, F. (2005), Variability in global land surface energy budgets during 1987–1988 simulated by an offline land surface model, *Clim. Dyn.*, *24*, 667–684, doi:10.1007/s00382-004-0439-4.

Chen, F., and J. Dudhia (2001), Coupling an advanced land-surface/hydrology model with the Penn State/NCAR MM5 modeling system. Part I: Model implementation and sensitivity, *Mon. Weather Rev.*, *129*, 569–585.

Chen, F., K. Mitchell, J. Schaake, Y. Xue, H. Pan, V. Koren, Y. Duan, M. Ek, and A. Betts (1996), Modeling of land-surface evaporation by four schemes and comparison with FIFE observations, *J. Geophys. Res.*, *101*, 7251–7268, doi:10.1029/95JD02165.

Chen, Y., and J. E. Penner (2005), Uncertainty analysis of the first indirect aerosol effect, *Atmos. Chem. Phys.*, *5*, 2935–2948.

Chou, M.-D., and M. Suarez (1994), An efficient thermal infrared radiation parameterization for use in general circulation models, NASA Tech. Mem. 104606, 3, Technical Report Series on Global Modeling and Data Assimilation, 85 pp.

Cui, Y. Y., A. Hodzic, J. N. Smith, J. Ortega, J. Brioude, H. Matsui, A. Turnipseed, P. Winkler, and B. de Foy (2014), Modeling ultrafine particle growth at a pine forest site influenced by anthropogenic pollution during BEACHON-RoMBAS 2011, *Atmos. Chem. Phys. Discuss.*, *14*, 5611–5651, doi:10.5194/acpd-14-5611-2014.

Cui, Z., S. Davies, K. S. Carslaw, and A. M. Blyth (2011), The response of precipitation to aerosol through riming and melting in deep convective clouds, *Atmos. Chem. Phys.*, *11*, 3495–3510.

Dusek, U., et al. (2006), Size matters more than chemistry for cloud-nucleating ability of aerosol particles, *Science*, *312*, 1375–1378, doi:10.1126/science.1125261.

Emmons, L. K., et al. (2010), Description and evaluation of the Model for Ozone and Related chemical Tracers, version 4 (MOZART-4), *Geosci. Model Dev.*, *3*, 43–67, doi:10.5194/gmd-3-43-2010.

Fan, J., T. Yuan, J. M. Comstock, S. Ghan, A. Khain, L. R. Leung, Z. Li, V. J. Martins and M. Ovchinnikov (2009), Dominant role by vertical wind shear in regulating aerosol effects on deep convective clouds, *J. Geophys. Res.*, *114*, D22206, doi:10.1029/2009JD012352.

Fan, J., J. M. Comstock, and M. Ovchinnikov (2010), The cloud condensation nuclei and ice nuclei effects on tropical anvil characteristics and water vapor of the tropical tropopause layer, *Environ. Res. Lett.*, *5*(4), 044005, doi:10.1088/1748-9326/5/4/044005.

Fast, J. D., W. I. Gustafson Jr., R. C. Easter, R. A. Zaveri, J. C. Barnard, E. G. Chapman, G. A. Grell, and S. E. Peckham (2006), Evolution of ozone, particulates, and aerosol direct radiative forcing in the vicinity of Houston using a fully coupled meteorology-chemistry-aerosol model, *J. Geophys. Res.*, *111*, D21305, doi:10.1029/2005JD006721.

Ghan, S. J., L. R. Leung, R. C. Easter, and H. Abdul-Razzak (1997), Prediction of cloud droplet number in a general circulation model, *J. Geophys. Res.*, *102*, 21,777–21,794, doi:10.1029/97JD01810.

Ghan, S. J., R. C. Easter, E. G. Chapman, K. Abdul-Razzak, Y. Zhang, L. R. Leung, N. S. Laulainen, R. D. Saylor, and R. A. Zaveri (2001), A physically based estimate of radiative forcing by anthropogenic sulfate aerosol, *J. Geophys. Res.*, *106*(D6), 5279–5293, doi:10.1029/2000JD900503.

Ghan, S. J., H. Abdul-Razzak, A. Nenes, Y. Ming, X. Liu, M. Ovchinnikov, B. Shipway, N. Meskhidze, J. Xu, and X. Shi (2011), Droplet nucleation: Physically-based parameterizations and comparative evaluation, *J. Adv. Model. Earth Syst.*, *3*, M10001, doi:10.1029/2011MS000074.

Grell, G. A., S. E. Peckham, R. Schmitz, S. A. McKeen, G. Frost, W. C. Skamarock, and B. Eder (2005), Fully coupled "online" chemistry within the WRF model, *Atmos. Environ.*, *39*, 6957–6975.

Guenther, A., T. Karl, P. Harley, C. Wiedinmyer, P. I. Palmer, and C. Geron (2006), Estimates of global terrestrial isoprene emissions using MEGAN (Model of Emissions of Gases and Aerosols from Nature), *Atmos. Chem. Phys.*, *6*, 3181–3210.

Heymsfield, A. J., A. Bansemer, G. Heymsfield, and A. O. Fierro (2009), Microphysics of maritime tropical convective updrafts at temperatures from 220° to 260°, *J. Atmos. Sci.*, *66*(12), 3530–3562, doi:10.1175/2009JAS3107.1.

Hong, S. Y., Y. Noh, and J. Dudhia (2006), A new vertical diffusion package with an explicit treatment of entrainment processes, *Mon. Weather Rev.*, *134*, 2318–2341.

Igel, A. L., S. C. van den Heever, C. M. Naud, S. M. Saleeby, and D. J. Posselt (2013), Sensitivity of warm-frontal processes to cloud-nucleating aerosol concentrations, *J. Atmos. Sci.*, *70*, 1768–1783.

Khain, A. P. (2009), Notes on state of the art investigations of aerosol effects on precipitation: A critical review, *Environ. Res. Lett.*, *4*, 015004, doi:10.1088/1748-9326/4/1/015004.

Khain, A., N. BenMoshe, and A. Pokrovsky (2008), Factors determining the impact of aerosols on surface precipitation from clouds: An attempt at classification, *J. Atmos. Sci.*, *65*, 1721–1748.
Koehler, K. A., S. M. Kreidenweis, P. J. DeMott, A. J. Prenni, and M. D. Petters (2007), Potential impact of Owens (dry) Lake dust on warm and cold cloud formation, *J. Geophys. Res.*, *112*, D12210, doi:10.1029/2007JD008413.
Kristjánsson, J. E. (2002), Studies of the aerosol indirect effect from sulfate and black carbon aerosols, *J. Geophys. Res.*, *107*(D15), 4246, doi:10.1029/2001JD000887.
Lebo, Z. J., and H. Morrison (2014), Dynamical effects of aerosol perturbations on simulated idealized squall lines, *Mon. Weather Rev.*, *142*, 991–1009, doi:10.1175/MWR-D-13-00156.1.
Lebo, Z. J., and J. H. Seinfeld (2011), Theoretical basis for convective invigoration due to increased aerosol concentration, *Atmos. Chem. Phys.*, *11*, 5407–5429, doi:10.5194/acp-11-5407-2011.
Lee, S. S., L. J. Donner, V. T. J. Phillips, and Y. Ming (2008), The dependence of aerosol effects on clouds and precipitation on cloud-system organization, shear and stability, *J. Geophys. Res.*, *113*, D16202, doi:10.1029/2007JD009224.
Levin, E. J. T., A. J. Prenni, M. D. Petters, S. M. Kreidenweis, R. S. Sullivan, S. A. Atwood, J. Ortega, P. J. DeMott, and J. N. Smith (2012), An annual cycle of size-resolved aerosol hygroscopicity at a forested site in Colorado, *J. Geophys. Res.*, *117*, D06201, doi:10.1029/2011JD016854.
Levin, E. J. T., A. J. Prenni, B. B. Palm, D. A. Day, P. Campuzano-Jost, P. M. Winkler, S. M. Kreidenweis, P. J. DeMott, J. L. Jimenez, and J. N. Smith (2014), Size-resolved aerosol composition and its link to hygroscopicity at a forested site in Colorado, *Atmos. Chem. Phys.*, *14*, 2657–2667, doi:10.5194/acp-14-2657-2014.
Li, Z., F. Niu, J. Fan, Y. Liu, D. Rosenfeld, and Y. Ding (2011), Long-term impacts of aerosols on the vertical development of clouds and precipitation, *Nat. Geosci.*, *4*, 888–894, doi:10.1038/ngeo1313.
Lin, Y. L., R. D. Farley, and H. D. Orville (1983), Bulk parameterization of the snow field in a cloud model, *J. Clim. Appl. Meteorol.*, *22*, 1065–1092.
Liu, C., K. Ikeda, G. Thompson, R. Rasmussen, and J. Dudhia (2011), High-resolution simulations of wintertime precipitation in the Colorado Headwaters Region: Sensitivity to physics parameterizations, *Mon. Weather Rev.*, *139*, 3533–3553, doi:10.1175/MWR-D-11-00009.1.
Liu, Y., P. H. Daum, and R. L. McGraw (2005), Size truncation effect, threshold behavior, and a new type of autoconversion parameterization, *Geophys. Res. Lett.*, *32*, L11811, doi:10.1029/2005GL022636.
Lohmann, U., J. Feichter, J. E. Penner, and W. R. Leaitch (2000), Indirect effect of sulfate and carbonaceous aerosols: A mechanistic treatment, *J. Geophys. Res.*, *105*(D10), 12,193–12,206, doi:10.1029/1999JD901199.
Lynn, B. H., A. P. Khain, J. Dudhia, D. Rosenfeld, A. Pokrovsky, and A. Seifert (2005), Spectral (Bin) microphysics coupled with a mesoscale model (MM5). Part II: Simulation of a CaPE rain event with a squall line, *Mon. Weather Rev.*, *133*, 59–71.
Matsui, H., M. Koike, Y. Kondo, N. Takegawa, A. Wiedensohler, J. D. Fast, and R. A. Zaveri (2011), Impact of new particle formation on the concentrations of aerosols and cloud condensation nuclei around Beijing, *J. Geophys. Res.*, *116*, D19208, doi:10.1029/2011JD016025.
Matsui, H., M. Koike, Y. Kondo, J. D. Fast, and M. Takigawa (2014), Development of an aerosol microphysical module: Aerosol Two-dimensional bin module for foRmation and Aging Simulation (ATRAS), *Atmos. Chem. Phys.*, *14*, 10,315–10,331, doi:10.5194/acp-14-10315-2014.
Mesinger, F., et al. (2006), North American regional reanalysis, *Bull. Am. Meteorol. Soc.*, *87*, 343–360.
Mlawer, E. J., S. J. Taubman, P. D. Brown, M. J. Iacono, and S. A. Clough (1997), Radiative transfer for inhomogeneous atmospheres: RRTM, a validated correlated-k model for the longwave, *J. Geophys. Res.*, *102*(D14), 16,663–16,682, doi:10.1029/97JD00237.
Morrison, H., and W. W. Grabowski (2011), Cloud-system resolving model simulations of aerosol indirect effects on tropical deep convection and its thermodynamic environment, *Atmos. Chem. Phys.*, *11*, 10,503–10,523, doi:10.5194/acp-11-10503-2011.
Morrison, H., and W. W. Grabowski (2013), Response of tropical deep convection to localized heating perturbations: Implications for aerosol-induced convective invigoration, *J. Atmos. Sci.*, *70*, 3533–3555, doi:10.1175/JAS-D-13-027.1.
Nguyen, T. K. V., M. D. Petters, S. R. Suda, and A. G. Carlton (2014), Trends in particle phase liquid water during the Southern Oxidant and Aerosol Study, *Atmos. Chem. Phys. Discuss.*, *14*, 7469–7516, doi:10.5194/acpd-14-7469-2014.
Ntelekos, A. A., J. A. Smith, L. Donner, J. D. Fast, W. I. Gustafson, E. G. Chapman, and W. F. Krajewski (2009), The effects of aerosols on intense convective precipitation in the northeastern United States, *Q. J. R. Meteorol. Soc.*, *135*, 1367–1391, doi:10.1002/qj.476.
Ortega, J., et al. (2014), Overview of the Manitou Experimental Forest Observatory: Site description and selected science results from 2008–2013, *Atmos. Chem. Phys. Discuss.*, *14*, 1647–1709, doi:10.5194/acpd-14-1647-2014.
Penner, J. E., J. Quaas, T. Storelvmo, T. Takemura, O. Boucher, H. Guo, A. Kirkevåg, J. E. Kristjánsson, and Ø. Seland (2006), Model intercomparison of indirect aerosol effects, *Atmos. Chem. Phys.*, *6*, 3391–3405, doi:10.5194/acp-6-3391-2006.
Petters, M. D., and S. M. Kreidenweis (2007), A single parameter representation of hygroscopic growth and cloud condensation nucleus activity, *Atmos. Chem. Phys.*, *7*, 1961–1971.
Petters, M. D., A. J. Prenni, S. M. Kreidenweis, and P. J. DeMott (2007), On measuring the critical diameter of cloud condensation nuclei using mobility selected aerosol, *Aerosol Sci. Technol.*, *41*, 907–913, doi:10.1080/02786820701557214.
Petters, M. D., C. M. Carrico, S. M. Kreidenweis, A. J. Prenni, P. J. DeMott, J. L. Collett Jr. and H. Moosmüller (2009), Cloud condensation nucleation activity of biomass burning aerosol, *J. Geophys. Res.*, *114*, D22205, doi:10.1029/2009JD012353.
Pinsky, M. B., and A. P. Khain (2002), Effects of in-cloud nucleation and turbulence on droplet spectrum formation in cumulus clouds, *Q. J. R. Meteorol. Soc.*, *128*, 501–533, doi:10.1256/003590002321042072.
Reutter, P., H. Su, J. Trentmann, M. Simmel, D. Rose, S. S. Gunthe, H. Wernli, M. O. Andreae, and U. Pöschl (2009), Aerosol- and updraft-limited regimes of cloud droplet formation: Influence of particle number, size and hygroscopicity on the activation of cloud condensation nuclei (CCN), *Atmos. Chem. Phys.*, *9*, 7067–7080, doi:10.5194/acp-9-7067-2009.
Roberts, G., and A. Nenes (2005), A continuous-flow streamwise thermal-gradient CCN chamber for atmospheric measurements, *Aerosol Sci. Technol.*, *39*, 206–221, doi:10.1080/027868290913988.
Rosenfeld, D., U. Lohmann, G. B. Raga, C. D. O'Dowd, M. Kulmala, S. Fuzzi, A. Reissell, and M. O. Andreae (2008), Flood or drought: How do aerosols affect precipitation?, *Science*, *321*, 1309–1313, doi:10.1126/science.1160606.
Segal, Y., M. Pinsky, A. Khain, and C. Erlick (2003), Thermodynamic factors influencing bimodal spectrum formation in cumulus clouds, *Atmos. Res.*, *66*, 43–64, doi:10.1016/S0169-8095(02)00172-2.
Segele, Z. T., L. M. Leslie, and P. J. Lamb (2013), Weather Research and Forecasting Model simulations of extended warm-season heavy precipitation episode over the US Southern Great Plains: Data assimilation and microphysics sensitivity experiments, *Tellus A*, *65*, 19,599, doi:10.3402/tellusa.v65i0.19599.
Seifert, A., and K. D. Beheng (2006), A two-moment cloud microphysics parameterization for mixed-phase clouds. Part 2: Maritime vs. continental deep convective storms, *Meteorol. Atmos. Phys.*, *92*, 67–82.
Seifert, A., C. Kohler, and K. D. Beheng (2012), Aerosol- cloud-precipitation effects over Germany as simulated by a convective scale numerical weather prediction model, *Atmos. Chem. Phys.*, *12*, 709–725.

Shaw, W., K. J. Allwine, B. G. Fritz, F. C. Rutz, J. P. Rishel, and E. G. Chapman (2008), An evaluation of the wind erosion module in DUSTRAN, *Atmos. Environ.*, *42*, 1907–1921.

Skamarock, W. C., J. B. Klemp, J. Dudhia, D. O. Gill, D. M. Barker, G. M. Duda, X.-Y. Huang, W. Wang, and J. G. Powers (2008), A description of the Advanced Research WRF Version 3, Boulder, CO, NCAR: 113 pp.

Sorooshian, A., G. Feingold, M. D. Lebsock, H. Jiang, and G. L. Stephens (2009), On the precipitation susceptibility of clouds to aerosol perturbations, *Geophys. Res. Lett.*, *36*, L13803, doi:10.1029/2009GL038993.

Stevens, B., and G. Feingold (2009), Untangling aerosol effects on clouds and precipitation in a buffered system, *Nature*, *461*, 607–613.

Tao, W.-K., J.-P. Chen, Z. Li, C. Wang, and C. Zhang (2012), Impact of aerosols on convective clouds and precipitation, *Rev. Geophys.*, *50*, RG2001, doi:10.1029/2011RG000369.

Teller, A., and Z. Levin (2006), The effects of aerosols on precipitation and dimensions of subtropical clouds: A sensitivity study using a numerical cloud model, *Atmos. Chem. Phys.*, *6*, 67–80.

Thompson, G., and T. Eidhammer (2014), A study of aerosol impacts on clouds and precipitation development in a large winter cyclone, *J. Atmos. Sci.*, *71*, 3636–3658, doi:10.1175/JAS-D-13-0305.1.

Twomey, S. (1974), Pollution and the planetary albedo, *Atmos. Environ.*, *8*, 1251–1256.

Van den Heever, S. C., G. G. Carrio, W. R. Cotton, P. J. DeMott, and A. J. Prenni (2006), Impacts of nucleating aerosol on Florida storms. Part I: Mesoscale simulations, *J. Atmos. Sci.*, *63*, 1752–1775.

Van den Heever, S. C., G. L. Stephens, and N. B. Wood (2011), Aerosol indirect effects on tropical convection characteristics under conditions of radiative-convective equilibrium, *J. Atmos. Sci.*, *68*, 699–718.

Wang, C. (2005), A model study of the response of tropical deep convection to the increase of CCN concentration: 1. Dynamics and microphysics, *J. Geophys. Res.*, *110*, D21211, doi:10.1029/2004JD005720.

Ward, D. S., T. Eidhammer, W. R. Cotton, and S. M. Kreidenweis (2010), The role of the particle size distribution in assessing aerosol composition effects on simulated droplet activation, *Atmos. Chem. Phys.*, *10*, 5435–5447.

Wexler, A., F. W. Lurmann, and J. H. Seinfeld (1994), Modeling urban and regional aerosols: 1. Model development, *Atmos. Environ.*, *28*, 531–546.

Zaveri, R. A., and L. K. Peters (1999), A new lumped structure photochemical mechanism for large-scale applications, *J. Geophys. Res.*, *104*, 30,387–30,415, doi:10.1029/1999JD900876.

Zaveri, R. A., R. C. Easter, J. D. Fast, and L. K. Peters (2008), Model for Simulating Aerosol Interactions and Chemistry (MOSAIC), *J. Geophys. Res.*, *113*, D13204, doi:10.1029/2007JD008782.

Zhang, Y., M. K. Dubey, S. C. Olsen, J. Zheng, and R. Zhang (2009), Comparisons of WRF/Chem simulations in Mexico City with ground-based RAMA measurements during the 2006-MILAGRO, *Atmos. Chem. Phys.*, *9*, 3777–3798, doi:10.5194/acp-9-3777-2009.

Zhao, Z., M. S. Pritchard, and L. M. Russell (2012), Effects on precipitation, clouds, and temperature from long-range transport of idealized aerosol plumes in WRF-Chem simulations, *J. Geophys. Res.*, *117*, D05206, doi:10.1029/2011JD016744.